Underestimation of Column NO_2 Amounts from the OMI Satellite Compared to Diurnally Varying Ground-Based Retrievals from Multiple Pandora Spectrometer Instruments

Jay Herman[1], Nader Abuhassan[1], Jhoon Kim[2], Jae Kim[3], Manvendra Dubey[4], Marcelo Raponi[5], Maria Tzortziou[6]

Abstract

Retrievals of Total Column NO_2 ($TCNO_2$) are compared for 14 sites from the Ozone Measuring Instrument (OMI using OMNO2-NASA v3.1) on the AURA satellite and from multiple ground-based PANDORA spectrometer instruments making direct-sun measurements. The result is that on a daily and monthly average basis, OMI almost always underestimates the amount $TCNO_2$ by 50 to 100%, while occasionally the daily OMI value exceeds that measured by PANDORA at very clean sites. In addition to systematic underestimates, OMI always misses the frequently much higher values of $TCNO_2$ that occur after the OMI overpass time. This suggests that OMI retrieved $TCNO_2$ are not suitable for air quality assessments as related to human health, especially in polluted urban areas. Six discussed Northern Hemisphere PANDORA sites have multi-year data records (Busan, Seoul, Washington DC, Waterflow New Mexico, Boulder Colorado, and Mauna Loa) and one site in the Southern Hemisphere (Buenos Aires Argentina). The first four of these sites and Buenos Aires frequently have high $TCNO_2$ ($TCNO_2$ > 0.5 DU). Eight additional sites have shorter term data records in the US and South Korea. One of these is a one-year data record from a highly polluted site at City College in New York City with pollution levels comparable to Seoul, South Korea. OMI estimated air mass factor, surface reflectivity, and the OMI 24x13 km^2 FOV (field of view) are three factors that can cause OMI to underestimate $TCNO_2$. Because of the local inhomogeneity of NO_2 emissions, the large OMI FOV is the most likely factor for consistent underestimates when comparing OMI $TCNO_2$ to retrievals from the small PANDORA effective FOV (measured in m^2) calculated from the solar diameter of 0.5^{O}.

Key Words: Nitrogen dioxide, OMI, PAN, PANDORA, ground-based, satellite

Correspondence email: jay.r.herman@nasa.gov

[1]University of Maryland Baltimore County JCET, Maryland
[2]Department of Atmospheric Sciences, Yonsei National University, South Korea
[3]Department of Atmospheric Science, Pusan National University, South Korea
[4]Earth Systems Observations, Los Alamos National Laboratory, Los Alamos, NM 87545
[5]Departamento de Investigaciones en Láseres y Aplicaciones (DEILAP), Instituto de Investigaciones Científicas y Técnicas para la Defensa (CITEDEF), Ministerio de Defensa (MINDEF), Buenos Aires, Argentina
[6]City College of New York, New York City, NY

Underestimation of Column NO_2 Amounts from the OMI Satellite Compared to Ground-Based Retrievals from Multiple Pandora Spectrometer Instruments

1.0 Introduction

Retrieval of Total Column NO_2 ($TCNO_2$) from the Ozone Monitoring Instrument (OMI) has been a scientific success story for the past 14 years. Near total global coverage from the well-calibrated OMI has enabled observation of all the regions where NO_2 is produced and has permitted monitoring of the changes during the 2004 to 2019 period, especially in regions where there is heavy and growing industrial activity (e.g., China and India). $TCNO_2$ amounts (data used: OMNO2-NASA v3.1) retrieved from OMI over various specified land locations show a strong underestimate compared to co-located Pandora Spectrometer Instruments (the abbreviation PAN is used for graph and table labels). The underestimate of OMI $TCNO_2$ at the overpass time compared to ground-based measurements has previously been reported at a few specific locations (Bechle, 2013; Lamsal et al., 2015; Ialongo et al., 2017; Kollonige, et al., 2018; Goldberg et al., 2018; Herman et al., 2018). For any location, the OMI overpass local standard time consists of the central overpass near the 13:30 hour equator crossing solar time and occasionally a side viewing overpass from adjacent orbits within ±90 minutes of the central overpass time. Independently from instrument calibration and retrieval errors, there are two specific aspects to the underestimation of $TCNO_2$ pollution levels. First, the mid-day OMI observations do not see the large diurnal variation of $TCNO_2$ that usually occur after the 13:30 overpass time, and second, because of spatial inhomogeneity the large OMI field of view (FOV) footprint 13 x 24 km^2 at OMI nadir view tends to average regions of high NO_2 amounts (Nowlan et al., 2016; Judd et al., 2018) with those from lower pollution areas. An analysis by Judd et al., (2019, their Fig. 9) shows the effect of decreasing satellite spatial resolution on improving agreement with PANDORA, with the best agreement occurring with an airborne instrument, GEO-TASO (resolution 3x3 km^2) followed by TropOMI (5x5 km^2) and then OMI (18x18 km^2). Both OMI and TropOMI show an underestimate of $TCNO_2$ compared to PANDORA.

There are other possible systematic retrieval errors with OMI $TCNO_2$. The largest of these is determining the air mass factor (AMF) needed to convert slant column measurements into vertical column amounts followed by the surface reflectivity Rs (Boersma et al., 2011; Lin et al., 2015; Nowlan et al., 2016; Lorente et al., 2018). Accurately determining the AMF for $TCNO_2$ requires a-priori knowledge of the NO_2 profile shape (Krotkov et al., 2017), which is estimated from coarse resolution model calculations (Boersma et al., 2011), and using the correct Rs. Currently Rs is found using a statistical process of sorting through years of data to find relatively clear-sky scenes for each location (Kleipool, et al., 2008; O'Byrne et al., 2010). Boersma et al., 2004 gave a detailed error analysis for the various components contributing OMI $TCNO_2$ retrievals resulting an estimated "retrieval precision of 35-60%" in heavily polluted areas dominated by determining the air mass factor. An improved V2.0 DOMINO retrieval (Boersma et al., 2011) algorithm reduced the retrieval errors while increasing the estimated airmass factor, which reduces the retrieved $TCNO_2$ up to 20% in winter and 10% in summer. The current version of OMNO2-NASA (Krotkov et al., 2017) and v2.0 DOMINO (Boersma et al., 2011) are generally in good agreement (Marchenko et al., 2015; Zara et al., 2018). However, the OMNO2-NASA $TCNO_2$ retrievals are 10 to 15% lower than the v2.0 DOMINO retrievals and with Quality Assurance for Essential Climate Variables (QA4ECV) retrievals. A subsequent detailed analysis of surface reflectivity (Vasilkov et al., 2017) shows that retrieval of $TCNO_2$ in highly polluted areas (e.g., some areas in China) can increase by 50% with the use of geometry-dependent reflectivities, but only increase about 5% in less polluted areas. For PANDORA, calculation of the solar viewing AMF is a simple geometric problem (AMF is approximately proportional to the cosecant of the solar zenith angle SZA) and is independent of R_S (Herman et al., 2009). For a polluted region with $TCNO_2$ = 5.34×10^{16} molecules/cm^2 or 2 DU, the PANDORA error is expected to be less than ±2.5% with the largest uncertainty coming from an assumed nominal amount of stratospheric $TCNO_2$ = 0.1 DU.

Accurate satellite $TCNO_2$ retrievals (and for other trace gases) are important in the estimate of the effect of polluted air containing NO_2 on human health (Kim and Song, 2017 and references therein), especially from the viewpoint of NO_2 as a respiratory irritant and precursor to cancer (Choudhari et al., 2013). Since NO_2 is largely produced by combustion, satellite observations of NO_2 serve as a proxy for changing industrial activity. Another important application requiring accurate measurements of the amount of $TCNO_2$ and its diurnal variation is atmospheric NO_2 contribution to nitrification of coastal waters (Tzortziou et al., 2018).

We show that the use of OMI $TCNO_2$ for estimating local air quality and coastal nitrification on a global basis is misleading for most polluted locations, and especially on days when the morning or afternoon amounts are higher than those occurring at the OMI overpass time near 13:30 hours standard time. OMI $TCNO_2$ data are extremely useful for estimating regional pollution amounts and for assessing long-term changes in these amounts. Modelling studies (Lamsal et al., 2017 Fig. 1) based on the Global Modelling Initiative model (Strahan et al., 2007) simulating $TCNO_2$ diurnal variation over Maryland USA (37-40^{O}N, 74-79^{O}W) shows a late afternoon peak and shows that the stratospheric component does not substantially contribute to this peak. Boersma et al. (2016) show that sampling strategy can cause systematic errors between OMI $TCNO_2$ and model $TCNO_2$ with satellite results being up to 20% lower than models. Duncan et al., (2014) reviews the applicability of satellite $TCNO_2$ data to represent air quality and notes that $TCNO_2$ correlates well with surface levels of NO_2 in industrial regions and states that the portion of $TCNO_2$ in the boundary layer could be over 75% of the total vertical column depending on NO_2 altitude profile shape.

This paper presents 14 different site comparisons between retrieved OMI $TCNO_2$ overpass values that are co-located with PANDORA $TCNO_2$ amounts from various locations in the world. Six of the comparisons are where PANDORAs have long-term data (1-year or longer) records. The comparisons are done using 80 second cadence data matched to the OMI overpass times averaged over ±6 minutes and with monthly running averages calculated using Lowess(f) (Locally Weighted least squares fit to a fraction f of the data points, (Cleveland, 1981) of OMI-PANDORA time matched $TCNO_2$. OMI overpass data, https://avdc.gsfc.nasa.gov/index.php?site=666843934&id=13, are filtered for the row anomaly and cloudy pixels. The selection of a ±6-minute window represents 720 seconds or 9 PANDORA measurements averaged together around the OMI overpass time to reduce the effect of outlier points. The specific value of ±6 minutes is arbitrary but increases the effective signal to noise ratio by a factor of 3. PANDORA data are filtered for significant cloud cover by examining the effective variance in sub-interval (20 seconds) measurements. Each PANDORA listed measurement is the average of up to 4000 (clear sky) individual measurement made over 20 seconds.

This paper gives a discussion and presentation of data on the effect of diurnal variation that are always missed at the local OMI mid-day overpass times. We show that OMI $TCNO_2$ values are also systematically lower than PANDORA values at sites with significant pollution ($TCNO_2 > 0.3$ DU). We present a unique view of a year of fully time resolved diurnal variation of $TCNO_2$ at two sites, Washington DC and New York City, which are similar to other polluted locations.

2.0 Brief Instrument Descriptions

For the purposes of $TCNO_2$ retrievals, both OMI and PANDORA are spectrometer-based instruments using nearly the same spectral range and similar spectral resolution (about 0.5 nm). Both use spectral fitting retrieval algorithms that differ (Boersma et al. 2011; Herman et al., 2009) because of the differences between direct-sun viewing retrievals (PANDORA) and above the atmosphere downward viewing retrievals (OMI). The biggest difference is with the respective fields of view, 13 x 24 km^2 at OMI nadir view and larger off-nadir FOV compared to the much smaller PANDORA FOV (1.2^{O}) measured in m^2 with the precise value depending on the NO_2 profile shape and the solar zenith angle. For example, if most of the $TCNO_2$ is located below 2 km, then the PANDORA FOV is approximately given by $(1.2\pi/180)(2/\cos(SZA))$, which for SZA = 45^{O} is about 59x59 m^2. If the solar disk (0.5^{O}) is used as the limiting factor, then the effective FOV is smaller (25x25 m^2).

2.1 OMI

OMI is an east-west side (2600 km) and nadir viewing polar orbiting imaging spectrometer that measures the earth's backscattered and reflected radiation in the range 270 to 500 nm with a spectral resolution of 0.5 nm. The polar orbiting side viewing capabilities produce a pole to pole swath that is about 2600 km wide displaced in longitude every 90 minutes by the earth's rotation to provide coverage of nearly the entire sunlit Earth once per day at a 13:30 solar hour equator crossing time with spatial gaps at low latitudes. OMI provides full global coverage every 2 to 3 days. Additional gaps are caused by a problem with the OMI CCD, "row anomaly" (Torres et al., 2018) that effectively reduces the number of near-nadir overpass views. A detailed OMI instrument description is given in Levelt et al. (2006). $TCNO_2$ is determined in the visible spectral range from 405 to 465 nm where the NO_2 absorption spectrum has the maximum spectral structure and where there is little interference from other trace gas species (there is a weak water feature in this range). OMI $TCNO_2$ overpass data are available for many ground sites (currently 719) from the following NASA website. https://avdc.gsfc.nasa.gov/index.php?site=666843934&id=13 (valid as of 16 July 2019).

2.2 PANDORA

PANDORA is a sun-viewing instrument for SZA < 80^{O} that obtains about 4000 spectra for clear-sky views of the sun in 20 seconds for each of two ranges UV (290 – 380 nm using a UV340 bandpass filter) and visible plus UV (280 – 525 nm using no filter). The overall measurement time is about 80 seconds including a 20 second dark-current measurements between each spectral measurement throughout the day. About 4000 clear-sky spectra for the UV and visible portions are separately averaged together to achieve very high signal to noise ratios (SNR). The UV340 filter for UV portion of the spectra reduces stray light effects from the visible wavelength range. A detailed description of PANDORA and its SNR is given in Herman et al., (2009; 2015). The effect of moderate cloud cover (reduction of observed signal by a factor of 8) in the PANDORA FOV on $TCNO_2$ retrievals is small (Herman et al., 2018). Cloud cover also reduces the number of measurements possible in 20 seconds, which potentially increases the noise level. PANDORA is driven by a highly accurate sun tracker that points an optical head at the sun and transmits the received light to an Avantes 2048 x 32 pixel CCD spectrometer (AvaSpec-ULS2048 from 280 – 525 nm with 0.6 nm resolution) through a 50 micron diameter fiber optic cable. The estimated $TCNO_2$ error is approximately 0.05 DU (1 DU = 2.69 x 10^{16} molecules cm^{-2}) out of a typical value of 0.3 DU in relatively clean areas and over 3 DU in highly polluted areas. PANDORA data are available for 250 sites. Some sites have multi-year data sets, but many of these sites are short-term campaign sites. https://avdc.gsfc.nasa.gov/pub/DSCOVR/Pandora/DATA_01/. (valid as of 16 July 2019).

3.0 Overpass Comparisons and Diurnal Variation of $TCNO_2$

The contribution of NO_2 to air quality at the Earth's surface is usually a proportional function of $TCNO_2$ that varies with the time of day and with the altitude profile shape (Lamsal et al., 2013; Bechle et al., 2013). Most of the NO_2 amount is usually located between 0 and 3 km altitude with a small amount of about 0.1±0.05 DU (Dirksen et al. 2011) in the upper troposphere and stratosphere. Because of the relatively short chemical lifetime, 3-4 hours (Liu et al., 2016), in the lower atmosphere, most of the NO_2 is located near (0 to 20 km) its sources (industrial activity, power generation, and automobile traffic). At higher altitudes or in the winter months, the life time of NO_2 is longer permitting transport over larger distances from its sources.

During the South Korean campaign (KORUS-AQ) in the spring of 2016 the diurnal variations of $TCNO_2$ vs days of the year DOY were determined for 6 sites (Herman et al., 2018), one of which is reproduced here (Fig. 1) for the city of Busan showing relatively low values of $TCNO_2$ in the morning (0.5 DU), moderately high values during the middle of the day (1.3 DU), and very high values on some of the afternoons (2 to 3 DU). Of these data, OMI only observes midday values near the 13:30 time marked on the Local_Time axis of Fig.1 thereby missing very high values (2 to 3 DU) that frequently occur later in the afternoon coinciding with times when people are outdoors returning from work.

In addition to missing the $TCNO_2$ diurnal variation, the OMI values are about half those observed by PANDORA (Fig. 2) at the OMI overpass time, so that using OMI values to estimate NO_2 pollution seriously underestimates the air quality problem even at midday. The shaded area in Fig.2 corresponds to the period covered in the KORUS-AQ campaign 7 April to 11 June 2016 shown in Fig. 1. An extended time series for Busan location is shown in Fig. 3.

Because of the different effective NO_2 FOV of PANDORA (measured in m^2) while tracking the moving sun position located in the heart of Busan (FOV distance d < 5 km for an SZA < 70^O used for $TCNO_2$ retrievals), both the daily (Fig. 3, left panel) and PANDORA monthly average variation (Fig. 3, right panel), obtained at the OMI overpass time, differs from the variation in the OMI $TCNO_2$ because of the much larger OMI FOV (13 x 24 km^2 at OMI nadir view) retrieval. Because of this, the OMI time series has low correlation (r^2 = 0.1) with the PANDORA time series.

The extended OMI vs PANDORA time series from 2012 – 2017 for Busan (Fig. 3) shows the same magnitude of differences seen during the KORUS-AQ period. A similar OMI vs PANDORA plot for total column ozone TCO_3 (Appendix Fig A1) shows good agreement between PANDORA and OMI indicating that the PANDORA instrument was operating and tracking the sun properly. Because the spatial variability of TCO_3, which is mostly in the stratosphere, is much less than for $TCNO_2$, the effect of different FOV's is minimized for ozone.

The same type of differences, $TCNO_2$(PAN) > $TCNO_2$(OMI), are seen at a wide variety of sites (e.g., see Fig.4) for Northern Hemisphere sites and one site in the Southern Hemisphere where PANDORA has an extended time series. Comparing extended Busan multi-year time series, some broad-scale correlation can be seen with peaks in February 2013, January 2014, and in 2016. The OMI data from Busan are different than data from many sites, since Busan is located very near the ocean causing a portion of the OMI FOV to be over the unpolluted ocean areas, whereas PANDORA is located inland (Pusan University) in an area of dense automobile traffic and quite near mountains capable of trapping air.

Figures 4 and 5 show a variety of different sites, ranging from the Mauna Loa Observatory location at 3.4 km (11,161 feet) on a relatively clean Hawaiian Island surrounded by ocean to a polluted landlocked semi-arid site at Waterflow, New Mexico near a power plant. All the sites considered show a significant underestimate of OMI $TCNO_2$. A summary of the monthly average underestimates is given in Tables 1 and 2. For some sites there is evident correlation between the two offset measurements. For example, the PANDORA at NASA Headquarters in Washington DC tracks the OMI measurement quite well on a monthly average basis with a correlation coefficient of r^2(mn) = 0.7 even though the daily correlation is low (r^2(dy) = 0.17). Other sites have only short periods of correlation and overall weak correlation (Table 1 showing daily, dy and monthly, mn, correlation coefficients for the graphs in Figures 4 and 5)

$TCNO_2$(PAN) comparisons with $TCNO_2$(OMI) from Mauna Loa Observatory (Fig. 4) are not those that might be expected, since the PANDORA observations are in an area where there are almost no automobile emissions and certainly no power plants, yet PAN > OMI and $TCNO_2$(PAN) values are large enough so that the pollution values (0.18 DU) are well above the stratospheric values (approximately 0.1 DU). OMI, which mainly measures values over the clean ocean, has an average value of 0.1 DU. The PANDORA values suggest upward airflow from the nearby circumferential ring road and resort areas. The Mauna Loa $TCNO_2$ values do not show any correlation with the recent increased volcanic activity at Mt. Kilauea after 2016. Recently, the original Mauna Loa PANDORA has been replaced. The new instrument's calibration will be reviewed before being added to the time series as part of a general data quality assurance program that is starting with the most recently deployed or upgraded PANDORA instruments at about 100 locations.

An interesting inland site is near the very small town of Waterflow, New Mexico (Fig. 4), where two power plants located near the PANDORA site ceased operation on December 30, 2013 (Lindenmaier et al., 2014). According to a quote from AZCentral Newspaper (Tuesday 31 December 2013) "Three coal-fired generators that opened in the 1960s near Farmington, N.M., closed Monday as part of a $182 million plan for Arizona Public Service Co. to meet environmental regulations, the utility reported". The $TCNO_2$ data suggests that the actual shutdown occurred near October 15, 2013. After the shutdown, air quality improved in the area with $TCNO_2$ decreasing from 0.4 DU to 0.28 DU. The remaining more efficient generators continued to produce smaller $N0_2$ emissions. These were shut down at the end of 2016 with little additional observed change in $TCNO_2$, since these boilers used NO_2 scrubbers (Dubey at al., 2018 in preparation). A nearby highway (Route 64) about 2 km from the PANDORA site has little automobile traffic.

Table 1 Values of $TCNO_2$ for PANDORA and OMI from monthly averages in Figs. 4 and 5

Name	Location (Lat, Lon)	PAN (DU)	OMI (DU)	r^2 (dy, mn)
Mauna Loa Hawaii	19.536°, -155.5762°	0.16	0.11	0.01, 0.30
NASA HQ Washington DC	38.882°, -77.01°	0.34	0.25	0.17, 0.70
Waterflow New Mexico[1]	36.797°, -108.48°	0.32	0.18	0.13, 0.52
Seoul South Korea	37.5644°, 126.934°	1.2	0.58	0.11, 0.06
Busan South Korea	35.2353°, 129.0825°	0.68	0.32	0.09, 0.10
Boulder Colorado	39.9909°, -105.2607°	0.27	0.17	0.04, 0.09
Buenos Aires Argentina	-34.5554°, -58.5062°	0.50	0.26	0.16, 0.08
Average		**0.49**	**0.27**	

Table 2 Average values of $TCNO_2$ for PANDORA and OMI for additional sites

Name	Location (Lat, Lon)	PAN (DU)	OMI (DU)
Essex Maryland	39.31083°, -76.47444°	0.30	0.28
Baltimore Maryland	39.29149°, -76.59646°	0.45	0.27
Fresno California	36.7854°, -119.7731°	0.42	0.17
Denver La Casa Colorado	39.778°, -105.006°	0.68	0.19
GIST[2]	35.226°,126.843°	0.42	0.20
HUFS[3]	37.338°,127.265°	0.61	0.51
City College New York City	40.8153°,-73.9505°	0.60	0.40
Average		**0.50**	**0.29**

[1]Waterflow, NM is listed for OMI data as Four Corners, NM, a nearby landmark
[2]Gwangju Institute of Science and Technology S. Korea
[3]Hankuk University Foreign Studies South Korea

Table 2 contains a summary of some sites that were part of short-term Discover-AQ campaigns in Maryland, Texas, California, and Colorado, two longer-term sites in South Korea, and one in New York City. Essex, Maryland is located on the Chesapeake Bay 10 km east of the center of Baltimore. The site is relatively clean (PAN = 0.3 DU) compared to the center of Baltimore (PAN = 0.45 DU), while OMI measures about the same amounts for both sites (0.28 and 0.27 DU) because the OMI FOV is larger than the distance between the two sites. The Houston Texas site contains 7 months of data from January to July 2013 with widespread NO_2 pollution permitting PANDORA and OMI to measure the same average values even though PANDORA observes episodes on many days when $TCNO_2$ exceeds 1.5 DU for short periods at times not observed by OMI. Observations in the small city of Fresno, California were during January when agricultural sources of NO_2 were at a minimum (Almaraz, 2018), but automobile traffic in the center of Fresno was significant. In this situation, PANDORA recorded the effect of automobile traffic while OMI averaged the city of Fresno and surrounding fallow agricultural areas. The Denver La Casa location is in the center of the city in an area with high amounts of local automobile traffic and near the Cherokee power generating plant. The result is a high level of average pollution (0.42 DU) while OMI measures both the city center and the surrounding relatively clean plains areas. The HUFS South Korean site is southeast of Seoul in a fairly isolated valley. However, Seoul and its surrounding areas are a widespread transported source of pollution so that both PANDORA and OMI measure elevated $TCNO_2$ amounts. In contrast, the PANDORA GIST site is on the outskirts of a small city in southwestern South Korea with significant traffic. The result is significant amounts of localized $TCNO_2$ (PANDORA = 0.42) surrounded by areas that produce little NO_2 leading to OMI observing a very clean 0.2 DU. The average of sites in the two tables are similar leading to ratios of PAN/OMI of 1.8 and 1.7 respectively. The estimated 50% increase in OMI retrievals of $TCNO_2$ from using the geometry-dependent reflectivity (Vasilkov, 2017) for the most polluted sites will narrow the disagreement with PANDORA. For example, OMI Seoul $TCNO_2$ may become 0.87 DU (PANDORA = 1.2 DU) and Buenos Aires 0.39 DU (PANDORA = 0.5 DU) still underestimating the amount of NO_2 pollution and missing the significant diurnal variation.

For the six sites shown, the average OMI underestimate of $TCNO_2$ is approximately a factor of 1.8 at the overpass time on a monthly average basis with occasional spikes that exceed this amount. The bias values range from 1.1 to 3.6, with higher biases tending to be associated with higher $TCNO_2$ values. The factor of 1.8 underestimate ignores the frequent large values of $TCNO_2$ at other times during the day (Fig. 7). In addition, averaging $TCNO_2$(PAN) over each entire day yields average values for the whole period that are 10 to 20% higher than just averaging over midday values that matched the OMI overpass time. Aside from the absolute magnitude, the short-term variations (over several months) are similar for both OMI and PANDORA although mostly not correlated. If correlation coefficients r^2 are generated from linear fits to scatter plots of $TCNO_2$ from OMI vs PANDORA, the correlation is mostly poor (Examples, r^2 =: Seoul 0.06, Mauna Loa 0.3 NASA HQ 0.7, see Figs. 4 and 5). Additional sites with shorter PANDORA time series of $TCNO_2$ show similar behavior.

Duncan et al. (2016) estimated trends from OMI $TCNO_2$ time series and found that the Seoul metropolitan area had a decrease of -1.5 ± 1.3 %/Year (2005 – 2014) consistent with OMI estimated change of –1.4 ± 1%/year (2012 -2018) in this paper. However, for the small area near Yonsei University, the decrease estimated from PANDORA is -5.8 ± 0.75 %/Year. Park (2019) estimates that metropolitan Seoul has decreased in population even as surrounding areas have increased population.

The average percent differences between OMI and PANDORA shown in Fig. 6 are relatively constant over time for each site with small changes over each multi-year observation period. The differences between OMI and PANDORA are provided by forming the percent differences of the daily $TCNO_2$ values (Fig. 6) in the form 100(OMI – PAN)/PAN. Also shown are the average percent differences and the linear fit slopes in percent change per year of the percent differences over the multi-year period. For example, the Boulder percent difference goes from -31% to -23% over 4 years. Of the six sites in shown in Fig. 6, two have statistically significant slopes, Seoul South Korea 2.1±0.5 %/Year and NASA Headquarters in Washington DC 3.4±0.9 %/Year at the 2σ level suggesting a significant area average increase in pollution compared to PANDORA's local values.

For some sites (see Fig. 6), PANDORA and OMI trends are the same (Waterflow, NM, Buenos Aires, and Mauna Loa) while the other 3 sites show significantly different trends (Boulder, NASA HQ, and Seoul).

The results for Busan (from Fig. 3) show a least squares average for the percent difference of -48 ± 0.8% for the 2012 – 2018 period with a slope of 6.8 ± 1%/Year. There is a decrease in the percent difference after October 2015 (Fig. 3) that is mainly from PANDORA seeing less $TCNO_2$ than during the 2012 – 2014 period. There is a gap in the Busan time series from July 2014 until April 2015 when the original PANDORA was replaced with a new instrument. The calibrations of both PANDORAS appear to be correct. Because of the break in the time series it is not clear whether there was a change in local conditions around Pusan University compared to the wide area observed by OMI.

3.1 Diurnal Variation at NASA HQ Washington DC

Figure 7 shows details of the daily diurnal variation of $TCNO_2$ on the roof of NASA Headquarters Washington, DC adjacent to a major cross-town highway (I695) for every day during each month of 2015 for local time vs DOY. The midday observing local standard time for OMI is marked for each graph.

The amount of $TCNO_2$ is mostly from the adjacent highway and the surrounding urban area with heavy traffic. The relatively moderate $TCNO_2$ values (0.4 to 0.8 DU) are probably a testament to the effectiveness of catalytic converters mandatory on all US automobiles in such a high traffic area (Bishop and Steadman, 2015).

Figure 8 contains the daily $TCNO_2$ diurnal variability vs DOY for each month measured by a PANDORA from the roof of a building on the CCNY (City College of New York) campus in the middle of Manhattan in New York City (NYC). From the values shown, the pollution levels are quite high, rivaling the pollution levels in Seoul, South Korea (see Fig. 5). OMI at its mid-day overpass time would detect some of the high-level pollution events, but miss many others occurring mostly in the afternoon. There are a significant number of days in all the months where the $TCNO_2$ levels appear to be low (e.g., blue color in July and October), but the blue color still represents significant pollution levels ($TCNO_2$(PAN) > 0.5 DU) that are small only compared to the peak values during the month ($TCNO_2$(PAN) > 1 DU). The highest amount of $TCNO_2$ recorded during 2018 was about 5DU on 13 July 2018 from 11:20 and 12:30 EST (a time with very light winds (1 km/hr) and moderate temperature (25^{O}C). There were many smaller peaks between 2 and 3 DU throughout the year. Extreme cases of high NO_2 amounts are frequently associated with the local meteorology indications of stagnant air (Harkey et al., 2015),

For both Washington DC (Fig. 7) and New York City (Fig. 8) there is strong day-to-day and month to month variability that depends on the local meteorological conditions (Seo et al., 2018; Zeng et al., 2015) and the amount of automobile traffic in the area (Andersen et al., 2011; Amin et al., 2017). High $TCNO_2$ events occur most often in the afternoon such that the OMI overpass near 13:30 would miss most high $TCNO_2$ events. Poor air quality affecting respiratory health would be improperly characterized by both the OMI average values being too low (Fig. 4) and by missing the extreme pollution events that occur frequently in the late afternoon. The high value of $TCNO_2$ that occurred on 5 August (2.2 DU) at 07:45 EST for Washington DC is not a retrieval error (SZA less than 70^O), but is a one-time anomaly in 2015 compared to more usual high values of 1.5 DU with an occasional spike to 2 DU. It should be noted that $TCNO_2$ does not accurately represent the NO_2 concentration at the surface, since it is mostly a measure of the amount in the lower 2 km. However, it is roughly proportional to the surface measurements close to the pollution sources (Bechle et al., 2013; Knepp et al., 2014) with the exact proportionality dependent on the profile shape near the ground.

Similar daily diurnal variation graphs of $TCNO_2$ (Figs. 7 and 8) could be shown for each site. However, the basic idea is the same for each site. OMI underestimates the amount of $TCNO_2$ because of its large FOV and misses most of the peak events at other times of the day. For some sites, such as Busan and Seoul, the peak values can reach 3 DU and above late in the afternoon, which are never seen by OMI (Herman et al., 2018).

Figure 9 for CCNY is similar to the graphs in Figs. 4 – 6 showing the relative behavior between PANDORA and OMI but including only OMI pixels that are at a distance D < 30 km from CCNY. The results are almost identical to those when D < 80 km. There is a period in March 2018 when OMI $TCNO_2$ slightly exceeded that measured by PANDORA. OMI with its large FOV may be seeing part of the chemically driven seasonal variation, while PANDORA is seeing a nearly constant source driven amount mostly from automobile traffic. For most days during 2018, PAN($TCNO_2$) > OMI($TCNO_2$) with the average value for PAN = 0.65 DU and for OMI = 0.45 DU (Fig. 9 Panel B). The percent difference plot shows that there is a systematic increase between PANDORA and OMI $TCNO_2$ from a value 10% to a value of 50%.

4.0 Summary

Examination of long-term $TCNO_2$ monthly average time series from OMI satellite and PANDORA ground-based observations show that OMI systematically underestimates the amount of NO_2 in the atmosphere by an average factor of 1.5 to 2 at the local OMI overpass time near the equator crossing time of 13:30±1:30. As shown in Fig. 6 for $TCNO_2$, 100(OMI – PAN)/PAN least squares mean underestimates are much larger than error estimates. These differences are reduced for the smaller pixel size TropOMI TCNO2 values (Judd et al.,2019). In addition, the PANDORA diurnal time series for every day during a year at each site (only two typical sites are shown in this paper, NYC and NASA-HQ) shows peaks in $TCNO_2$ that are completely missed by only observing at mid-day. The result is that estimates of air quality related to health effects from OMI observations are strongly underestimated almost everywhere as shown at all the sites with a long PANDORA record. In comparisons to PANDORA, OMI data are mostly uncorrelated or weakly correlated (e.g., Seoul correlation coefficient r^2 = 0.06, Mauna Loa r^2 = 0.3), while NASA HQ in Washington, DC shows a correlation on a seasonal basis (NASA HQ r^2 = 0.7) suggesting a wide area coordinated source of NO_2 (most likely automobile traffic). The data from CCNY shows some correlation between the locations of the peaks and troughs. Seven short term $TCNO_2$ time series were examined showing similar results (Table 1), except when the pollution region is widespread as in the Seoul South Korea region. The conclusion is that while OMI satellite $TCNO_2$ data are uniquely able to assess regional long-term trends in $TCNO_2$ and provide a measure of the regional distribution of pollutants, the OMI data cannot properly assess local air quality or the effect on human health over extended periods in urban or industrial areas. This will continue to be the case, but to a lesser degree, when the OMI $TCNO_2$ data are improved by reprocessing with a new geometry-dependent reflectivity (Vasilkov, 2017) and by the smaller FOV of TropOMI. The analysis shows that locating PANDORAs at polluted sites could provide quantitative corrections for spatial and temporal biases that affect the determination of local air quality from satellite data. Satellite detection of diurnal variation of $TCNO_2$ will be improved with the upcoming launch of three planned geostationary satellites over Korea, US, and Europe To verify the proper operation of the various PANDORA instruments a similar analysis for Total Column Ozone TCO was performed (see Appendix) and shows close agreement between OMI and PANDORA, with the largest difference occurring for Mauna Loa Observatory at 3.4 km altitude, where PANDORA misses the ozone between the surface and 3.4 km.

Appendix

A1 Ozone This section shows the corresponding PANDORA total column ozone (TCO) values compared to OMI TCO for Busan South Korea (Fig. A1) that shows close agreement for the entire 2012 – 2017 period. The different fields of view for OMI and PANDORA have a much smaller effect because of the greater spatial uniformity of stratospheric ozone compared to tropospheric NO_2. Additional sites are summarized in Table A1. The largest TCO difference (15 DU or 5.6%) occurs for Mauna Loa Observatory (Altitude = 3.4 km) compared to OMI (Average altitude = Sea Level). The close results show that the PANDORA was working properly and pointing accurately at the sun. The PANDORA TCO data shown here use a mid-latitude effective ozone temperature correction from model calculations that may not be accurate of each individual site (Herman et al., 2017). The ozone retrievals shown here use an average effective ozone temperature instead of a locally measured ozone temperature (Herman et al., 2015;2017).

Table A1 Average values of TCO_3 for PANDORA and OMI

Location	PAN (DU)	OMI (DU)	Percent Difference
Mauna Loa Observatory Hawaii (3.394 km)*	254	269	5.6
NASA HQ Washington DC (0.02 km)	308	314	1.9
Waterflow New Mexico (1.64 km)	293	292	0.3
Yonsei University Seoul South Korea (0.07 km)	317	325	2.5
Busan University Busan South Korea(0.03 km)	313	315	0.6
Boulder, Colorado (NOAA Bldg) (1.617 km)	299	302	1.0
Buenos Aires, Argentina (0.025 km)	279	284	1.8
Essex, Maryland (0.012 km)	299	301	0.7
Baltimore, Maryland (0.01 km)	296	296	0.0
Fresno, California (0.939 km)	306	309	1.0
Denver La Casa Colorado (1.6 km)	292	294	0.7
Gwangju Institute of Science and Technology (GIST) S. Korea (0.021 km)	302	307	1.6
Hankuk University Foreign Studies (HUFS) South Korea (0.04 km)	318	326	2.5
City College Manhattan New York City (0.04 km)	316	325	2.8
Average	**299**	**304**	**1.6**

Acknowledgement: This project is supported by the Korea Ministry of Environment (MOE) as Public Technology Program based on Environmental Policy (2017000160001), by the Los Alamos National Laboratory's Laboratory Directed Research and Development program and by the NASA Pandora project managed by Dr. Robert Swap.

References

Almaraz, Maya,Edith Bai, Chao Wang, Justin Trousdel, Stephen Conley, Ian Faloona and Benjamin Z. Houlton, Agriculture is a major source of NOx pollution in California, SCIENCE ADVANCES,31, DOI:10.1126/sciadv.aao3477, 2018.

Amin, Md. Shohel Reza, Umma Tamima, and Luis Amador Jimenez, "Understanding Air Pollution from Induced Traffic during and after the Construction of a New Highway: Case Study of Highway 25 in Montreal," Journal of Advanced Transportation, vol. 2017, Article ID 5161308, 14 pages, 2017. https://doi.org/10.1155/2017/5161308, 2017.

Andersen, M. Hvidberg, S.S. Jensen, M. Ketzel, S. Loft, M. Sørensen, A. Tjønneland, K. Overvad, O. Raaschou-Nielsen Chronic obstructive pulmonary disease and long-term exposure to traffic-related air pollution: A cohort study, Am. J. Respir. Crit. Care Med., 183, pp. 455-461, 10.1164/rccm.201006-0937OC, 2011.

Bechle, M. J.; Millet, D. B.; Marshall, J. D. Remote sensing of exposure to NO2: Satellite versus ground-based measurement in a large urban area. Atmos. Environ., 69, 345-353, 2013

Bishop, Gary A. and Donald H. Stedman, Reactive Nitrogen Species Emission Trends in Three Light-/Medium-Duty United States Fleets, *Environmental Science & Technology* 2015 *49* (18), 11234-11240, DOI: 10.1021/acs.est.5b02392, 2015.

Boersma, K. F., H. J. Eskes, E. J. Brinksma, Error analysis for tropospheric NO_2 retrieval from space, J. Geophys. Res. Atmos., https://doi.org/10.1029/2003JD003962, 2004.

Boersma, K. F., Eskes, H. J., Dirksen, R. J., van der A, R. J., Veefkind, J. P., Stammes, P., Huijnen, V., Kleipool, Q. L., Sneep, M., Claas, J., Leitão, J., Richter, A., Zhou, Y., and Brunner, D.: An improved tropospheric NO_2 column retrieval algorithm for the Ozone Monitoring Instrument, Atmos. Meas. Tech., 4, 1905-1928, https://doi.org/10.5194/amt-4-1905-2011, 2011.

Boersma, K. F., Vinken, G. C. M., & Eskes, H. J., Representativeness errors in comparing chemistry transport and chemistry climate models with satellite UV–Vis tropospheric column retrievals. Geoscientific Model Development, 9(2), 875-898, 2016.

Choudhari, Sheetal Korde, Minal Chaudhary, Sachin Bagde, Amol R Gadbai and Vaishali Joshi, Nitric oxide and cancer: a review, World Journal of Surgical Oncology 2013, 11:118, http://www.wjso.com/content/11/1/118, 2013.

Cleveland, William S., *LOWESS: A program for smoothing scatterplots by robust locally weighted regression. The American Statistician.* ***35*** *(1): 54.* JSTOR 2683591. doi:10.2307/2683591, *1981.*

Dirksen, Ruud J., K. Folkert Boersma, Henk J. Eskes, Dmitry V. Ionov, Eric J. Bucsela, Pieternel F. Levelt, Hennie M. Kelder, Evaluation of stratospheric NO2 retrieved from the Ozone Monitoring Instrument: Intercomparison, diurnal cycle, and trending, J. Geophys. Res., 116, https://doi.org/10.1029/2010JD014943, 2011.

Duncan, B. N., L. N. Lamsal, A. M. Thompson, Y. Yoshida, Z. Lu, D. G. Streets, M. M. Hurwitz, and K. E. Pickering, A space-based, high-resolution view of notable changes in urban NOx pollution around the world (2005–2014), J. Geophys. Res. Atmos.,121, 976–996, doi:10.1002/2015JD024121, 2016.

Goldberg, D. L., Saide, P. E., Lamsal, L. N., de Foy, B., Lu, Z., Woo, J.-H., Kim, Y., Kim, J., Gao, M., Carmichael, G., and Streets, D. G.: A top-down assessment using OMI NO2 suggests an underestimate in the NOx emissions inventory in Seoul, South Korea during KORUS-AQ, Atmos. Chem. Phys. Discuss., https://doi.org/10.5194/acp-2018-678, in review, 2018.

Harkey, M., Holloway, T., Oberman, J., and Scotty, E., An evaluation of CMAQ NO2 using observed chemistry-meteorology correlations, J. Geophys. Res. Atmos., 120, 11,775– 11,797, doi:10.1002/2015JD023316, 2015.

Herman, J., A. Cede, E. Spinei, G. Mount, M. Tzortziou, and N. Abuhassan, NO2 column amounts from ground-based Pandora and MFDOAS spectrometers using the direct-sun DOAS technique: Intercomparisons and application to OMI validation, J. Geophys. Res., 114, D13307, doi:10.1029/2009JD011848, 2009.

Herman, J.R., R.D. Evans, A. Cede, N.K. Abuhassan, I. Petropavlovskikh, and G. McConville**,** Comparison of Ozone Retrievals from the Pandora Spectrometer System and Dobson Spectrophotometer in Boulder Colorado, Atmos. Meas. Tech., 8, 3407–3418, 2015 doi:10.5194/amt-8-3407-2015.

Herman, J., Evans, R., Cede, A., Abuhassan, N., Petropavlovskikh, I., McConville, G., Miyagawa, K., and Noirot, B.: Ozone comparison between Pandora #34, Dobson #061, OMI, and OMPS in Boulder, Colorado, for the period December 2013–December 2016, Atmos. Meas. Tech., 10, 3539-3545, https://doi.org/10.5194/amt-10-3539-2017, 2017.

Herman, J., Spinei, E., Fried, A., Kim, J., Kim, J., Kim, W., Cede, A., Abuhassan, N., and Segal-Rozenhaimer, M.: NO_2 and HCHO measurements in Korea from 2012 to 2016 from Pandora spectrometer instruments compared with OMI retrievals and with aircraft measurements during the KORUS-AQ campaign, Atmos. Meas. Tech., 11, 4583-4603, https://doi.org/10.5194/amt-11-4583-2018, 2018.

Ialongo, I., Herman, J., Krotkov, N., Lamsal, L., Boersma, K. F., Hovila, J., and Tamminen, J.: Comparison of OMI NO_2observations and their seasonal and weekly cycles with ground-based measurements in Helsinki, Atmos. Meas. Tech., 9, 5203-5212, https://doi.org/10.5194/amt-9-5203-2016, 2016.

Judd, Laura M., Jassim A. Al-Saadi, Lukas C. Valin, R. Bradley Pierce, Kai Yang, Scott J. Janz, Matthew G. Kowalewski, James J. Szykman, Martin Tiefengraber, and Moritz Mueller, The Dawn of Geostationary Air

Quality Monitoring: Case Studies From Seoul and Los Angeles, Environ. Sci.,https://doi.org/10.3389/fenvs.2018.00085, 2018.

Judd, L. M., Al-Saadi, J. A., Janz, S. J., Kowalewski, M. G., Pierce, R. B., Szykman, J. J., Valin, L. C., Swap, R., Cede, A., Mueller, M., Tiefengraber, M., Abuhassan, N., and Williams, D.: Evaluating the impact of spatial resolution on tropospheric NO_2 column comparisons within urban areas using high-resolution airborne data, Atmos. Meas. Tech. Discuss., https://doi.org/10.5194/amt-2019-161, in review, 2019.

Kleipool, Q.L., M.R. Dobber, J.F. De Haan and P.F. Levelt, Earth Surface Reflectance Climatology from Three Years of OMI Data, Journal of Geophysical Research, 113, doi:10.1029/2008JD010290, 2008.

Knepp, T., M. Pippin, J. Crawford, Jim Szykman, R. Long, L. Cowen, A. Cede, N. Abuhassan, J. Herman, R. Delgado, J. Compton, T. Berkoff, J. Fishman, D. Martins, R. Stauffer, A. Thompson, A. Weinheimer, D. Knapp, D. Montzka, D. Lenschow, AND D. Neil. Estimating Surface NO2 and SO2 Mixing Ratios from Fast-Response Total Column Observations and Potential Application to Geostationary Missions. JOURNAL OF ATMOSPHERIC CHEMISTRY. Springer, New York, NY, 0(0):1-26, (2014).

Kollonige, D. E., Thompson, A. M.,Josipovic, M., Tzortziou, M., Beukes, J. P.,Burger, R., … Laakso, L. (2018). OMI satellite and ground-based Pandora observations and their application to surface NO2 estimations at terrestrial and marine sites. Journal of Geophysical Research: Atmospheres, 123, 1441–1459. https://doi.org/10.1002/2017JD026518, 2018.

Krotkov, N. A., Lamsal, L. N., Celarier, E. A., Swartz, W. H., Marchenko, S. V., Bucsela, E. J., Chan, K. L., Wenig, M., and Zara, M.: The version 3 OMI NO_2 standard product, Atmos. Meas. Tech., 10, 3133-3149, https://doi.org/10.5194/amt-10-3133-2017, 2017.

Lamsal, L & Martin, Randall & Parrish, David & Krotkov, Nickolay., Scaling Relationship for NO_2 Pollution and Urban Population Size: A Satellite Perspective. Environmental science & technology. 47. 10.1021/es400744g, 2013.

Lamsal, L. N., Krotkov, N. A., Celarier, E. A., Swartz, W. H., Pickering, K. E., Bucsela, E. J., Martin, R. V., Philip, S., Irie, H., Cede, A., Herman, J., Weinheimer, A., Szykman, J. J., and Knepp, T. N.: Evaluation of OMI operational standard NO_2 column retrievals using in situ and surface-based NO_2 observations, Atmos. Chem. Phys. Discuss., 14, 14519-14573, doi:10.5194/acpd-14-14519-2014, 2014.

Lamsal, L. N., S. J. Janz, N. A. Krotkov, K. E. Pickering, R. J. D. Spurr, M. G. Kowalewski, C. P. Loughner, J. H. Crawford, W. H. Swartz, and J. R. Herman, High-resolution NO_2 observations from the Airborne Compact Atmospheric Mapper Retrieval and validation, J. Geophys. Res. Atmos., 122, 1953–1970, doi:10.1002/2016JD025483, 2017

Levelt, P. F., Van den Oord, G. H. J., Dobber, M. R., Malkki, A., Visser, H., de Vries, J., Stammes, P., Lundell, J. O. V., and Saari, H.: The Ozone Monitoring Instrument, IEEE T. Geosci. Remote, 44, 1093–1101, doi:10.1109/tgrs.2006.872333, 2006.

Lindenmaier, Rodica, Manvendra K. Dubey, Bradley G. Henderson, Zachary T. Butterfield, Jay R. Herman, Thom Rahn · S.-H. Lee, Multiscale observations of CO2, (CO2)-C-13, and pollutants at Four Corners for emission verification and attribution, Proceedings of the National Academy of Sciences 06/2014; 111(23):8386-8391. DOI:10.1073/pnas.132188311, 2014

Liu, F., Beirle, S., Zhang, Q., Dörner, S., He, K., and Wagner, T.: NO_x lifetimes and emissions of cities and power plants in polluted background estimated by satellite observations, Atmos. Chem. Phys., 16, 5283-5298, https://doi.org/10.5194/acp-16-5283-2016, 2016.

Lorente, A., Boersma, K. F., Stammes, P., Tilstra, L. G., Richter, A., Yu, H., Kharbouche, S., and Muller, J.-P.: The importance of surface reflectance anisotropy for cloud and NO_2 retrievals from GOME-2 and OMI, Atmos. Meas. Tech., 11, 4509-4529, https://doi.org/10.5194/amt-11-4509-2018, 2018.

Nowlan, C. R., Liu, X., Leitch, J. W., Chance, K., González Abad, G., Liu, C., Zoogman, P., Cole, J., Delker, T., Good, W., Murcray, F., Ruppert, L., Soo, D., Follette-Cook, M. B., Janz, S. J., Kowalewski, M. G., Loughner, C. P., Pickering, K. E., Herman, J. R., Beaver, M. R., Long, R. W., Szykman, J. J., Judd, L. M., Kelley, P., Luke, W. T., Ren, X., and Al-Saadi, J. A.: Nitrogen dioxide observations from the Geostationary Trace gas and Aerosol Sensor Optimization (GeoTASO) airborne instrument: Retrieval algorithm and measurements during DISCOVER-AQ Texas 2013, Atmos. Meas. Tech., 9, 2647-2668, https://doi.org/10.5194/amt-9-2647-2016, 2016.

O'Byrne, G., R. V. Martin,A. van Donkelaar, J. Joiner, and E. A. Celarier, Surface reflectivity from the Ozone Monitoring Instrument using the Moderate Resolution Imaging Spectroradiometer to eliminate clouds: Effects of snow on ultraviolet and visible trace gas retrievals, J. Geophys. Res., VOL. 115, D17305, doi:10.1029/2009JD013079, 2010.

Marchenko, S., N. A. Krotkov, L. N. Lamsal, E. A. Celarier, W. H. Swartz, and E. J. Bucsela, Revising the slant column densityretrieval of nitrogen dioxide observed by the Ozone Monitoring Instrument, J. Geophys. Res. Atmos., 120, 5670–5692, doi:10.1002/2014JD022913, 2015

Park, Se Hoon, Seoul, The Wiley Blackwell Encyclopedia of Urban and Regional Studies. Edited by Anthony Orum. John Wiley & Sons Ltd. Published 2019 by John Wiley & Sons Ltd. DOI: 10.1002/9781118568446.eurs0283, 2019.

Raponi, Marcelo, Cede, A, Santana Diaz, Daniel, Sanchez, R, A. Otero, L, O. Salvador, J, R. Ristori, P, Quel, Eduardo. Total Column Ozone Measured In Buenos Aires Between March And November 2017, Using A Pandora Spectrometer System. Anales AFA. 29(2), 46-50. 10.31527/analesafa.2018.29.2.46, 2018.

Seo, J., Park, D.-S. R., Kim, J. Y., Youn, D., Lim, Y. B., and Kim, Y.: Effects of meteorology and emissions on urban air quality: a quantitative statistical approach to long-term records (1999–2016) in Seoul, South Korea, Atmos. Chem. Phys., 18, 16121-16137, https://doi.org/10.5194/acp-18-16121-2018, 2018.

Torres, O., Bhartia, P. K., Jethva, H., and Ahn, C.: Impact of the ozone monitoring instrument row anomaly on the long-term record of aerosol products, Atmos. Meas. Tech., 11, 2701-2715, https://doi.org/10.5194/amt-11-2701-2018, 2018.

Tzortziou, M.; Parker, O.; Lamb, B.; Herman, J.R.; Lamsal, L.; Stauffer, R.; Abuhassan, N. Atmospheric Trace Gas (NO_2 and O_3) Variability in South Korean Coastal Waters, and Implications for Remote Sensing of Coastal Ocean Color Dynamics. *Remote Sens.*, *10*, 1587, ; doi:10.3390/rs10101587, 2018.

Vasilkov, A., Qin, W., Krotkov, N., Lamsal, L., Spurr, R., Haffner, D., Joiner, J., Yang, E.-S., and Marchenko, S.: Accounting for the effects of surface BRDF on satellite cloud and trace-gas retrievals: a new approach based on geometry-dependent Lambertian equivalent reflectivity applied to OMI algorithms, Atmos. Meas. Tech., 10, 333-349, https://doi.org/10.5194/amt-10-333-2017, 2017.

Zara, M., Boersma, K. F., De Smedt, I., Richter, A., Peters, E., van Geffen, J. H. G. M., Beirle, S., Wagner, T., Van Roozendael, M., Marchenko, S., Lamsal, L. N., and Eskes, H. J.: Improved slant column density retrieval of nitrogen dioxide and formaldehyde for OMI and GOME-2A from QA4ECV: intercomparison, uncertainty characterization, and trends, Atmos. Meas. Tech., 11, 4033-4058, https://doi.org/10.5194/amt-11-4033-2018, 2018.

Zheng, G. J., Duan, F. K., Su, H., Ma, Y. L., Cheng, Y., Zheng, B., Zhang, Q., Huang, T., Kimoto, T., Chang, D., Pöschl, U., Cheng, Y. F., and He, K. B.: Exploring the severe winter haze in Beijing: the impact of synoptic weather, regional transport and heterogeneous reactions, Atmos. Chem. Phys., 15, 2969–2983, https://doi.org/10.5194/acp-15-2969-2015, 2015.

Figure Captions

Fig 1 Diurnal variation of $TCNO_2$ measured at Pusan University in Busan South Korea

Fig. 2. Monthly average values of $TCNO_2$ for OMI and PANDORA at OMI overpass times

Fig. 3 Extended time series for Busan. Left Panel: individual matching PANDORA and OMI data points for the overpass time ± 6 minutes. Right Panel: monthly averages.

Fig. 4. PANDORA compared to OMI. Extended $TCNO_2$ overpass time series for Mauna Loa Observatory, Hawaii, NASA Headquarters, Washington DC, and Waterflow, New Mexico.

Fig. 5. PANDORA compared to OMI. Extended $TCNO_2$ overpass time series for Seoul South Korea, Boulder, Colorado, and Buenos Aires, Argentina (Raponi et al. 2018).

Fig. 6 Percent differences between OMI and PANDORA. The slopes are the absolute change in the percent difference. For example, the Boulder percent difference goes from -31% to -23% over 4 years. The LS Means are least squares means with the corresponding error estimates

Fig. 7A $TCNO_2$ diurnal variation (DU) from January to June, NASA Headquarters Washington, DC from January 2015 to June 2015. The approximate OMI overpass time near 13:30 hours is marked.

Fig. 7B $TCNO_2$ diurnal variation (DU) from July to December, NASA Headquarters Washington, DC from July 2015 to December 2015. The approximate OMI overpass time near 13:30 hours is marked

Fig. 8A $TCNO_2$ diurnal variation (DU) at CCNY in New York City January to June 2018. The approximate OMI overpass time near 13:30 hours is marked.

Fig. 8B $TCNO_2$ diurnal variation at CCNY in New York City July to December 2018. The peak near 5 DU occurs on 13 July 2018 between 11:20 and 12:30 EST. The approximate OMI overpass time near 13:30 hours is marked.

Fig. 9 $TCNO_2$ overpass time series for CCNY in Manhattan, New York City. Panel A: OMI overpass $TCNO_2$ (Black) compare with OMI (Red). Panel B: Monthly Lowess(0.08) fit to the daily overpass data. Panel C: Percent difference 100(OMI – PAN)/PAN calculated from the data in Panel A

Fig. A1 Monthly average values of TCO for OMI and PANDORA at OMI overpass times for Busan South Korea

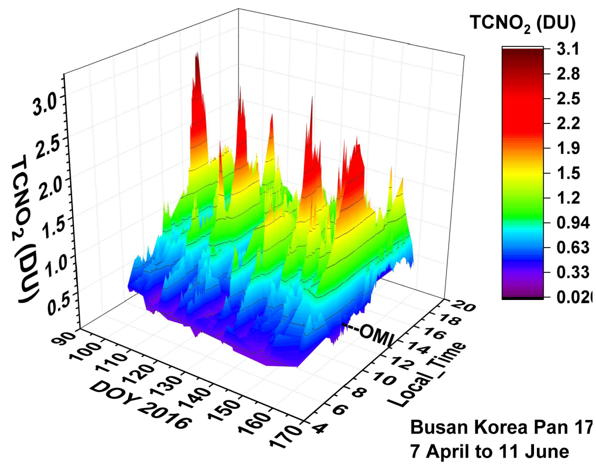

Fig 1 Diurnal variation of $TCNO_2$ measured at Pusan University in Busan South Korea

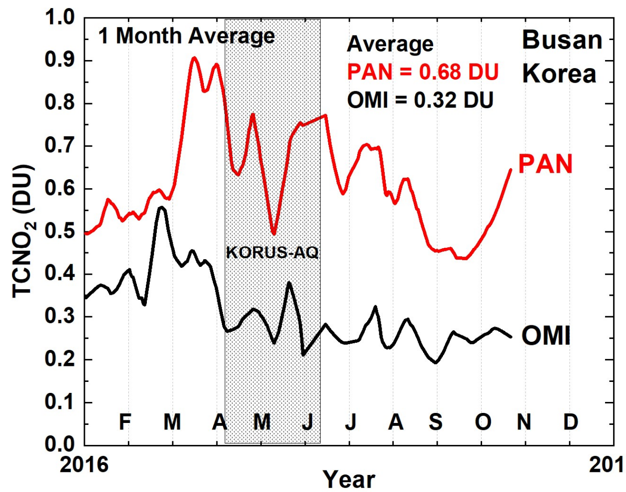

Fig. 2. Monthly average values of $TCNO_2$ for OMI and PANDORA at OMI overpass times

FIGURE 1 **FIGURE 2**

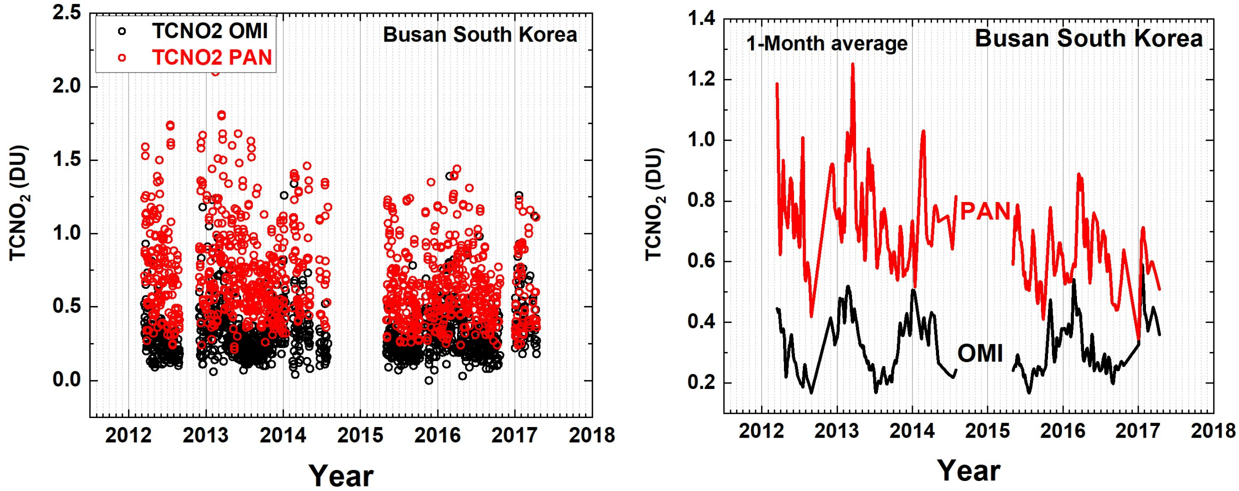

Fig. 3 Extended time series for Busan. Left Panel: individual matching PANDORA and OMI data points for the overpass time ± 6 minutes. Right Panel: monthly averages.

FIGURE 3

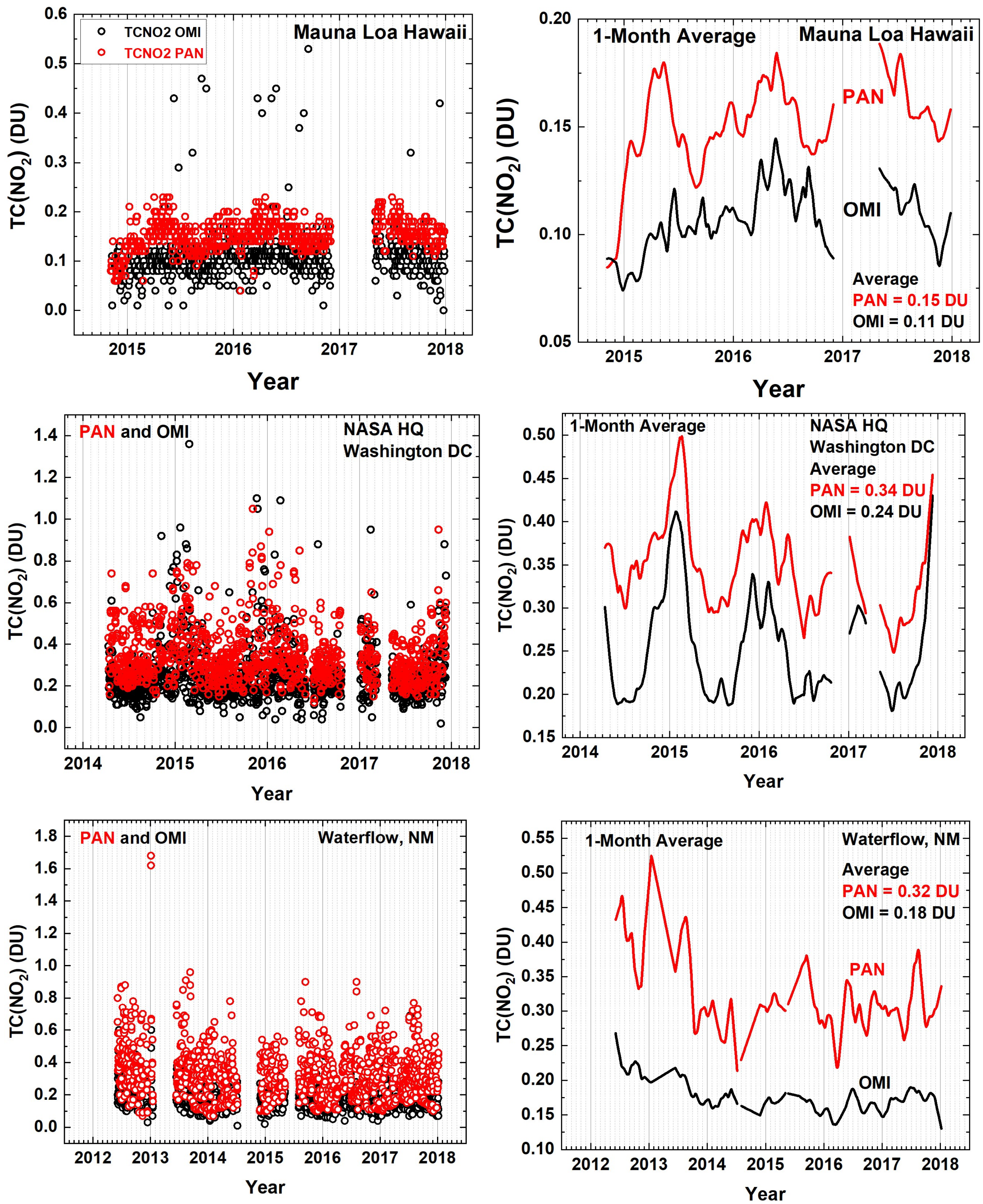

Fig. 4. PANDORA compared to OMI. Extended $TCNO_2$ overpass time series for Mauna Loa Observatory, Hawaii, NASA Headquarters, Washington DC, and Waterflow, New Mexico.

FIGURE 4

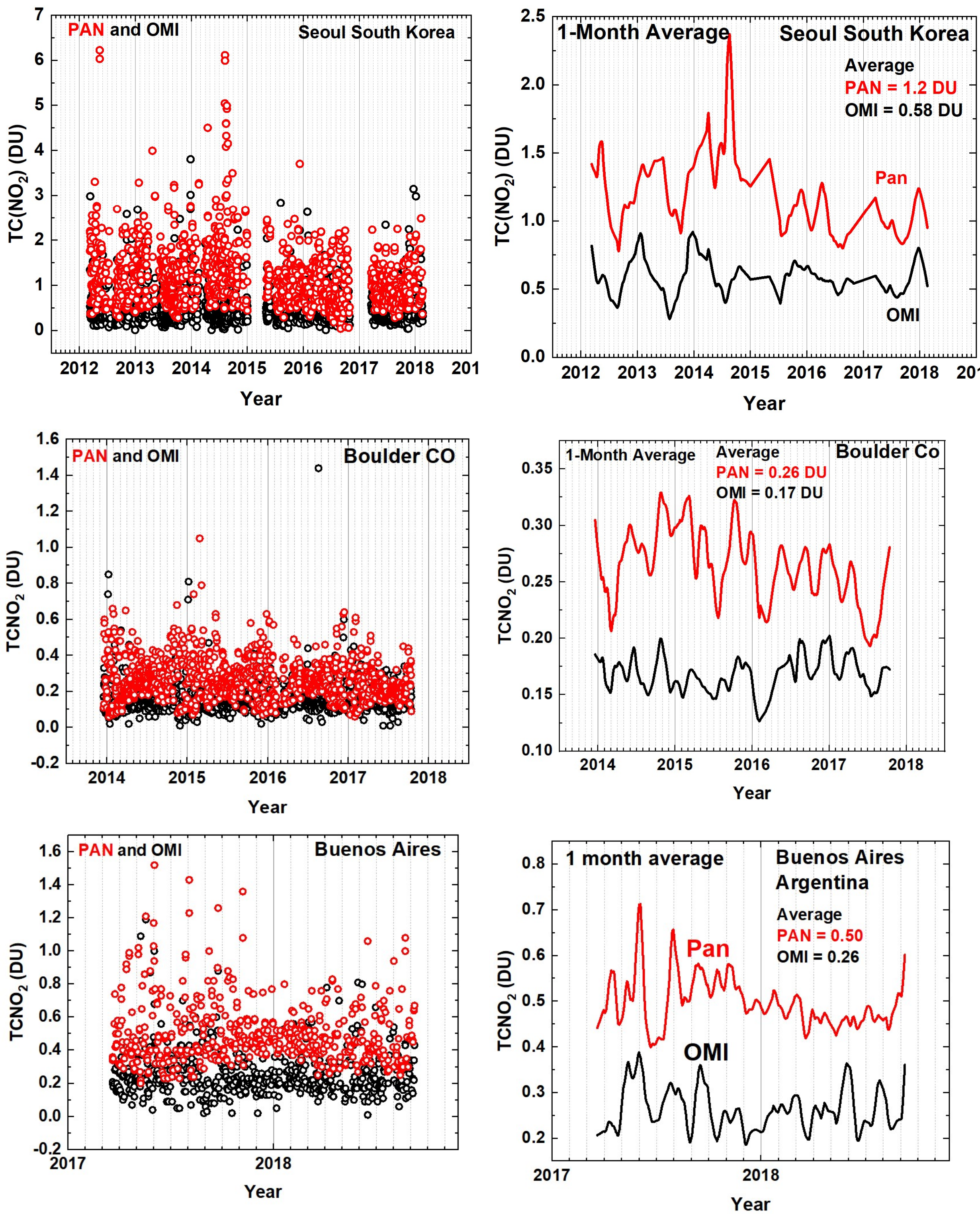

Fig. 5. PANDORA compared to OMI. Extended $TCNO_2$ overpass time series for Seoul South Korea, Boulder, Colorado, and Buenos Aires, Argentina (Raponi et al. 2017).

FIGURE 5

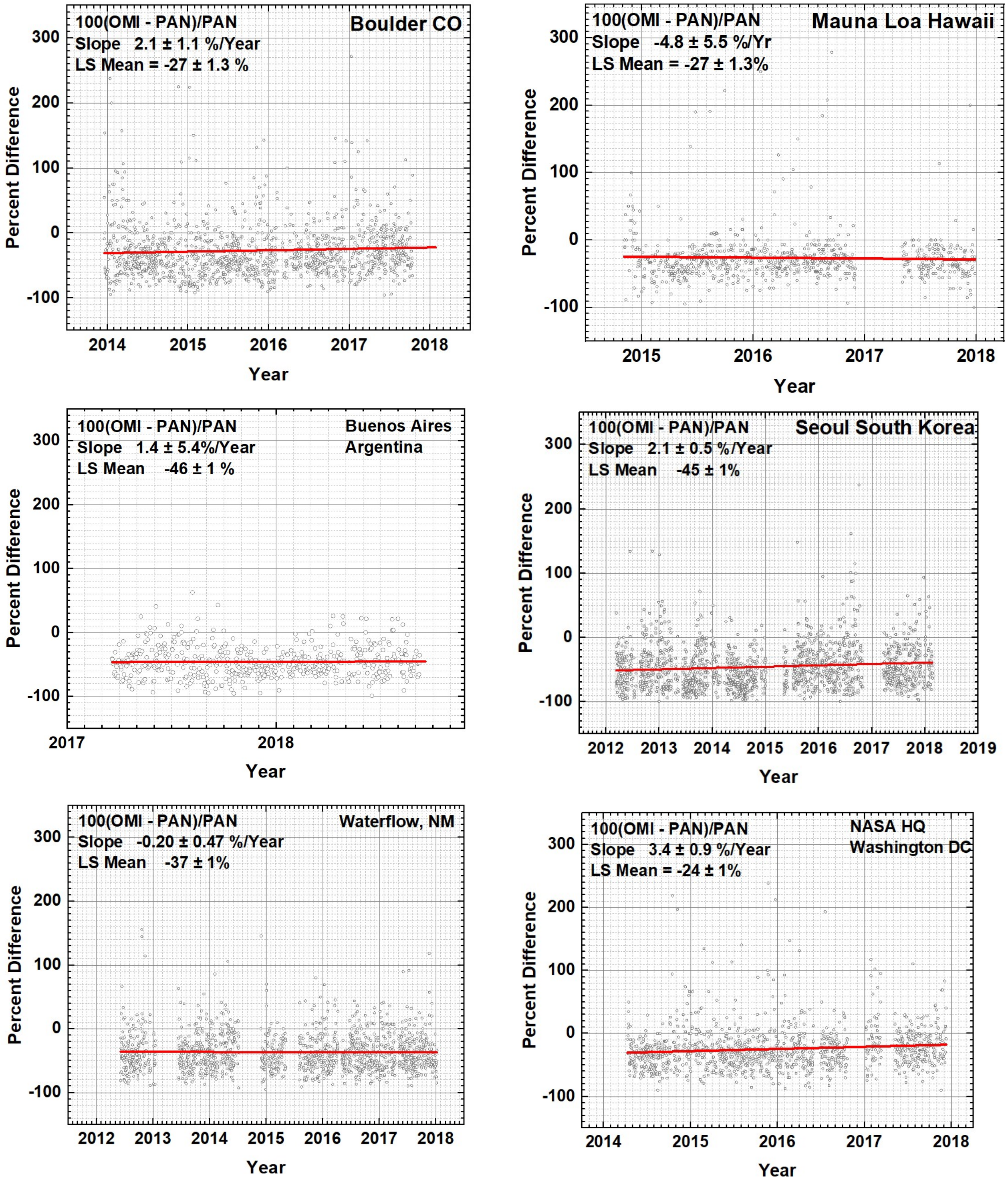

Fig. 6 Percent differences between OMI and PANDORA. The slopes are the absolute change in the percent difference. For example, the Boulder percent difference goes from -31% to -23% over 4 years. The LS Means are least squares means with the corresponding error estimates

FIGURE 6

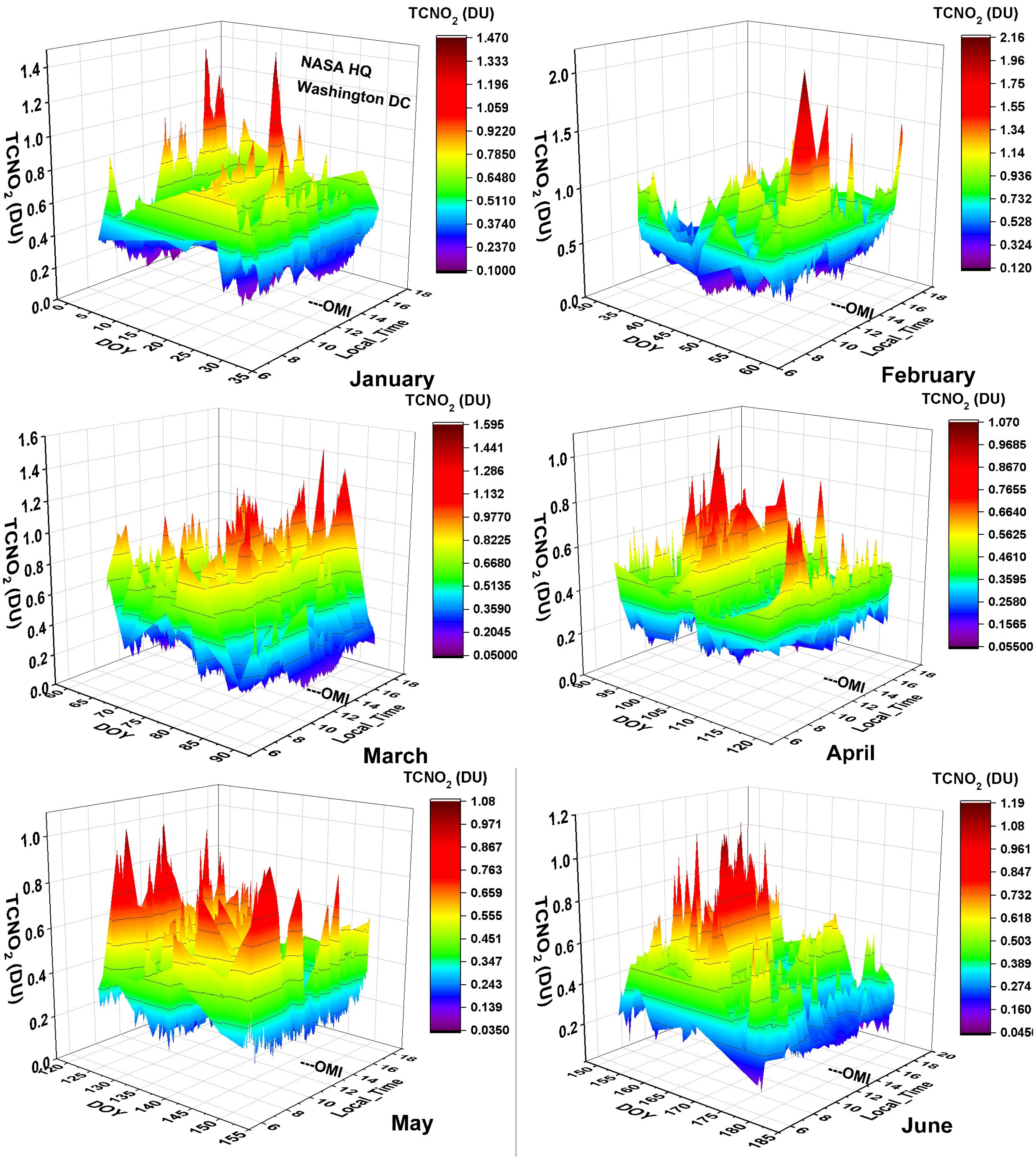

Fig. 7A $TCNO_2$ diurnal variation (DU) from January to June, NASA Headquarters Washington, DC from January 2015 to June 2015. The approximate OMI overpass time near 13:30 hours is marked

FIGURE 7A

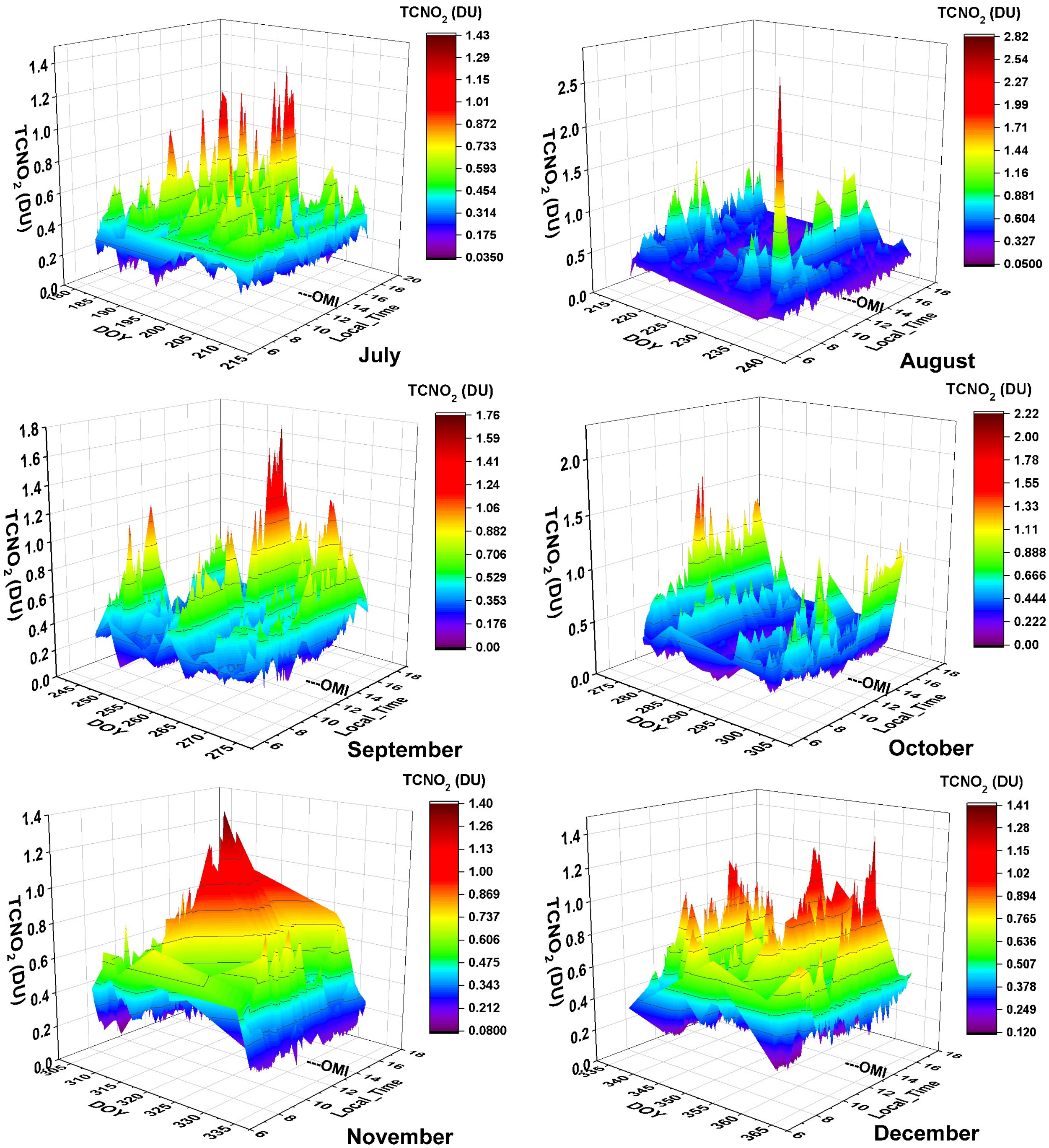

Fig. 7B $TCNO_2$ diurnal variation (DU) from July to December, NASA Headquarters Washington, DC from July 2015 to December 2015. The approximate OMI overpass time near 13:30 hours is marked

FIGURE 7B

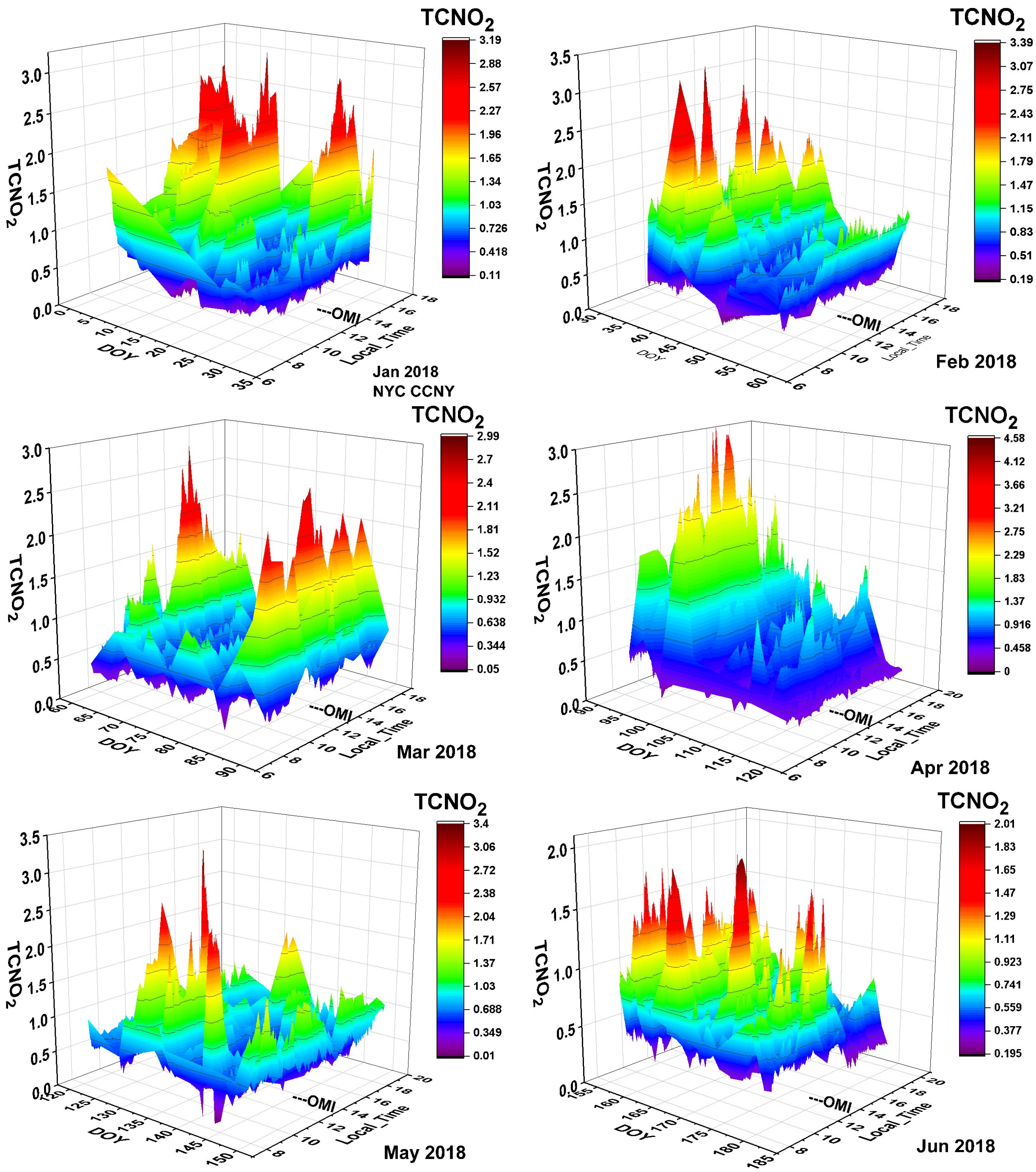

Fig. 8A $TCNO_2$ diurnal variation (DU) at CCNY in New York City January to June 2018. The approximate OMI overpass time near 13:30 hours is marked

Figure 8A

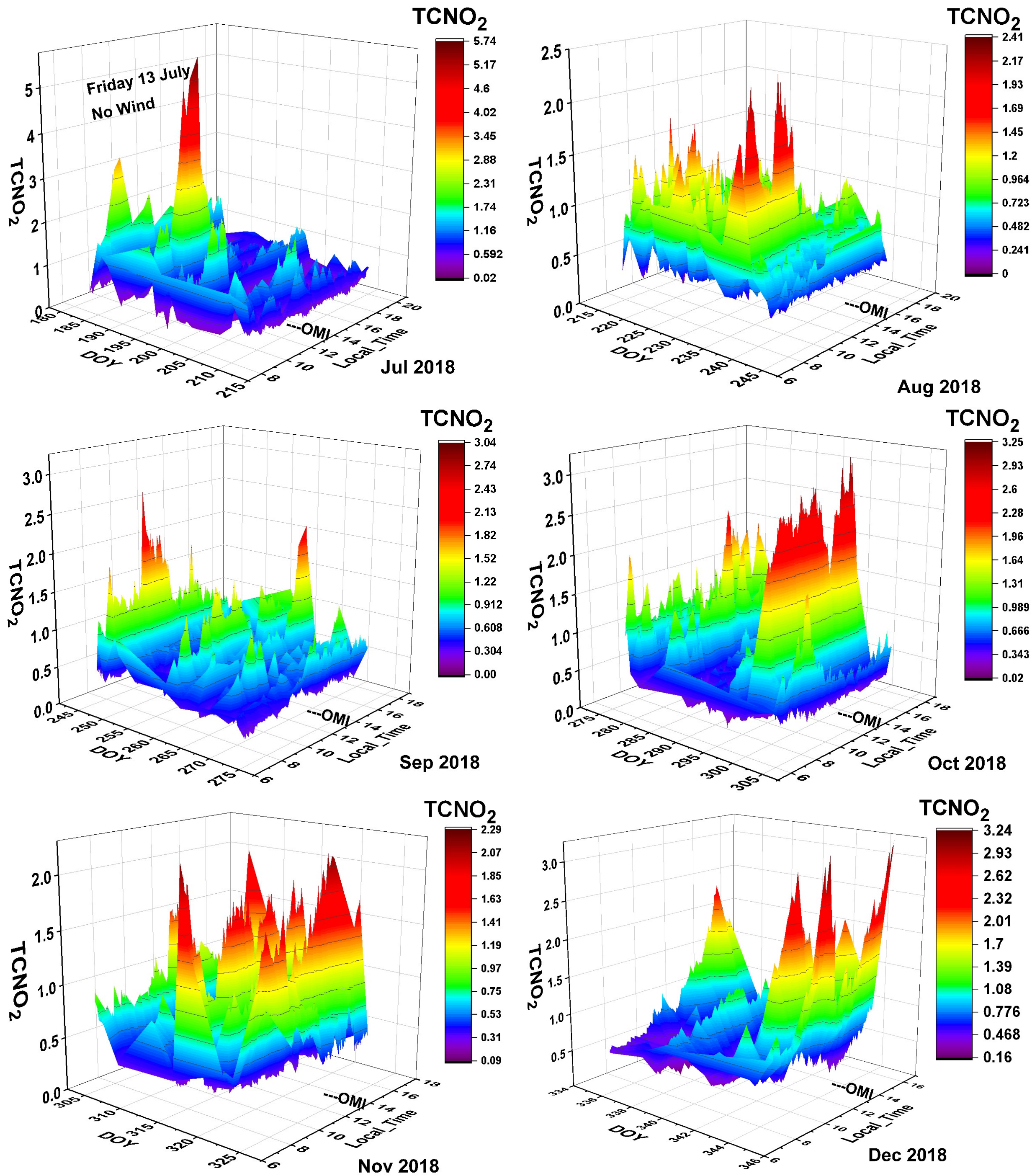

Fig. 8B $TCNO_2$ diurnal variation (DU) at CCNY in New York City July to December 2018. The peak near 5 DU occurs on 13 July 2018 between 11:20 and 12:30 EST. The approximate OMI overpass time near 13:30 hours is marked.

Figure 8B

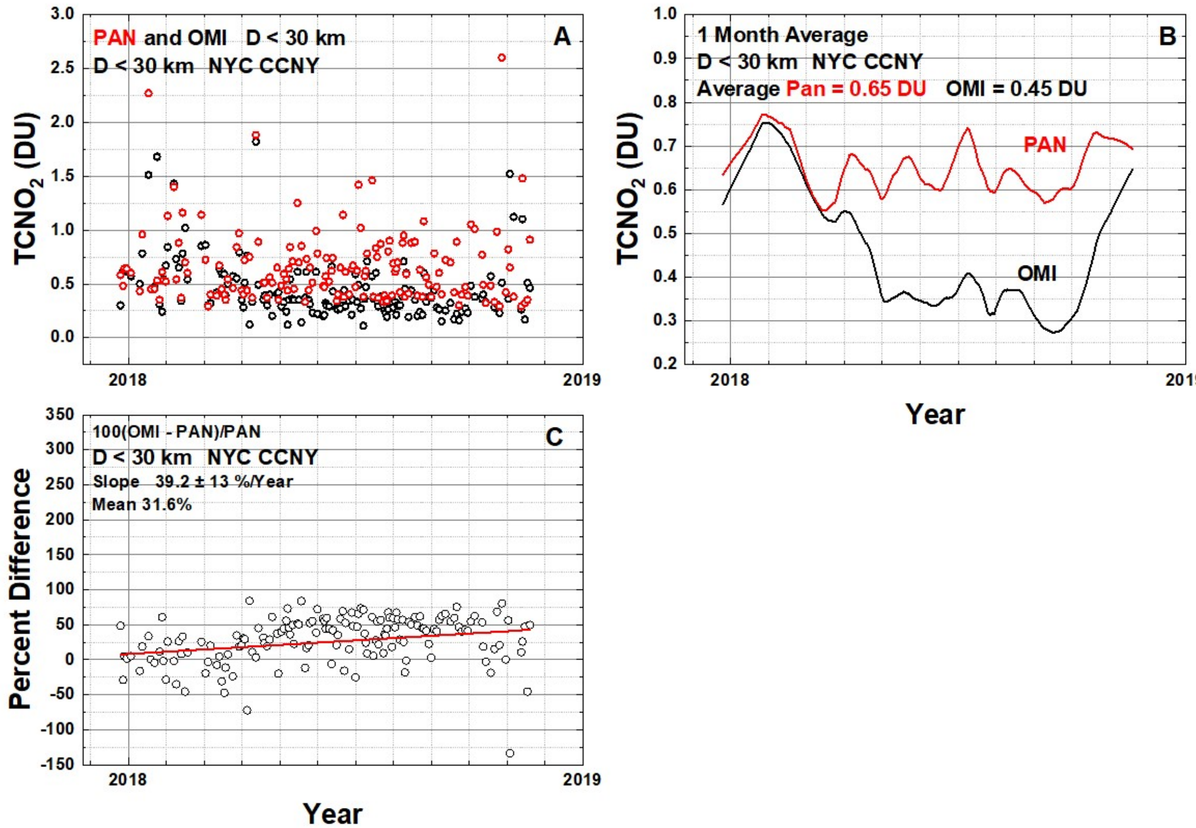

Fig. 9 $TCNO_2$ overpass time series for CCNY in Manhattan, New York City. OMI pixels are at a distance D < 30 km from CCNY. Panel A: OMI overpass $TCNO_2$ (Black) compare with OMI (Red). Panel B: Monthly Lowess(f) fit to the daily overpass data. Panel C: Percent difference 100(OMI – PAN)/PAN calculated from the data in Panel A

Figure 9

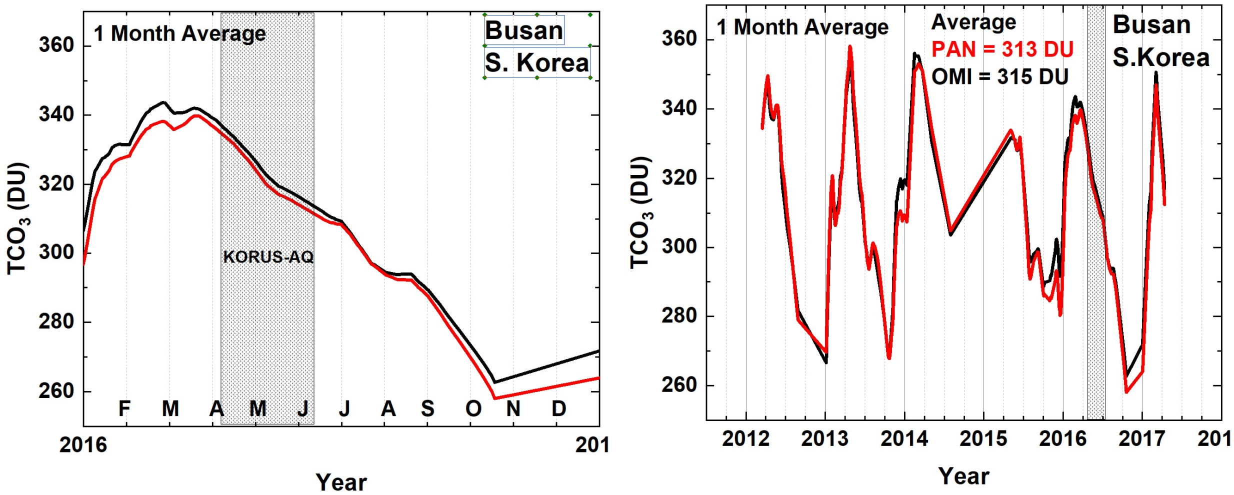

Fig. A1 Monthly average values of TCO_3 for OMI and PANDORA at OMI overpass times for Busan South Korea

FIGURE A1